

# Molecular Line Observations of a Carbon-Chain-Rich Core L492

Tomoya HIROTA

*National Astronomical Observatory of Japan,*

*Osawa 2-21-1, Mitaka, Tokyo 181-8588, Japan; tomoya.hirota@nao.ac.jp*

and

Satoshi YAMAMOTO

*Department of Physics and Research Center for the Early Universe,*

*The University of Tokyo, Bunkyo-ku, Tokyo 113-0033, JAPAN*

## ABSTRACT

We report on molecular abundances and distributions in a starless dense core L492. We have found that the abundances of carbon-chain molecules such as CCS, C<sub>3</sub>S, HC<sub>3</sub>N, HC<sub>5</sub>N, and HC<sub>7</sub>N are comparable to those in chemically young dark cloud cores called "carbon-chain-producing regions", such as L1495B, L1521B, L1521E, and TMC-1. This is the first dark cloud core with extremely rich in carbon-chain-molecules that is found outside the Taurus region. In addition, the deuterium fractionation ratios of DNC/HNC and DCO<sup>+</sup>/HCO<sup>+</sup> are also comparable to those in carbon-chain-producing regions, being significantly lower than those in the evolved prestellar cores such as L1498 and L1544. On the other hand, the abundances of NH<sub>3</sub> and N<sub>2</sub>H<sup>+</sup> are systematically higher than those in carbon-chain-producing regions. Our mapping observations reveal that the central hole of molecular distributions, which were reported for CCS and C<sup>34</sup>S in evolved prestellar cores is not significant in L492, indicating that the depletion factor of molecules is not very high. Furthermore, L492 is dynamically more evolved than carbon-chain-producing regions, and the protostellar collapse has started like L1498 and L1544. Therefore, it is likely that the chemical and dynamical evolutionary stage of L492 is intermediate between carbon-chain-producing regions (L1495B, L1521B, L1521E, and TMC-1) and evolved prestellar cores (L1498 and L1544).

*Subject headings:* ISM:abundances — ISM:individual(L492) — ISM:Molecules — radio lines: ISM

## 1. Introduction

In the last decade, special attention has been paid to starless cores or prestellar cores in dark clouds in order to investigate initial conditions of protostellar collapse. Since the detection of infalling motion in a prestellar core L1544 in the Taurus Molecular Cloud (Myers et al. 1996), a number of observational studies on L1544 and similar prestellar cores such as L1498 in the Taurus Molecular Cloud have been carried out with molecular lines and dust continuum emission (e.g. Tafalla et al. 2002, 2004). One of the most interesting features found in L1498 and L1544 is an evidence of molecular depletion in the central part of the cores (e.g. Kuiper et al. 1996; Ohashi et al. 1999; Caselli et al. 2002b). Both observational and theoretical studies reveal that abundances of CO, CS, and CCS are depleted in the chemically evolved cores, while  $\text{NH}_3$  and  $\text{N}_2\text{H}^+$  are not (Bergin & Langer 1997; Aikawa et al. 2005). These studies have promoted understanding of chemical properties as well as kinematics of evolved prestellar cores just under the collapsing phase.

Although detailed studies on evolved prestellar cores were extensively carried out, no systematic studies on younger cores have been made for a long time, except for TMC-1 (e.g. Hirahara et al. 1992, 1995; Pratap et al. 1997). It is because most of dense cores observed in the previous studies were based on the catalog of Benson & Myers (1989), which are prepared by the  $\text{NH}_3$  observations. On the other hand, Suzuki et al. (1992) pointed out that  $\text{NH}_3$  is not always a good tracer of dense cores because of the chemical abundance variation from core to core. They found anticorrelation between abundances of  $\text{NH}_3$  and carbon-chain-molecules such as CCS,  $\text{HC}_3\text{N}$ , and  $\text{HC}_5\text{N}$ , and identified a few starless cores where the carbon-chain molecules are abundant while  $\text{NH}_3$  is deficient. They are L1495B, L1521B, L1521E, and the cyanopolyne peak of TMC-1, and are called "carbon-chain-producing regions". Chemical model calculations suggest that the carbon-chain-producing regions are in the early stage of chemical evolution while dense cores traced by the  $\text{NH}_3$  lines are rather evolved (Suzuki et al. 1992; Bergin & Langer 1997).

In order to investigate basic physical and chemical properties of carbon-chain-producing regions, we carried out detailed observations of L1521E (Hirota et al. 2002), L1495B and L1521B (Hirota et al. 2004). For each of these three regions, we found a compact dense core traced by the  $\text{H}^{13}\text{CO}^+$ , CCS,  $\text{C}_3\text{S}$ , and  $\text{HC}_3\text{N}$  lines and their distributions have a single peak at the same position. Such a distribution is different from those in evolved prestellar cores, L1498 and L1544. In addition, abundances of  $\text{NH}_3$  and  $\text{N}_2\text{H}^+$  are extremely lower in these three regions than in other prestellar cores, while those of carbon-chain-molecules are systematically higher. According to our survey of deuterated molecules, deuterium fractionation ratios of  $\text{DNC/HNC}$  and  $\text{DCO}^+/\text{HCO}^+$  are systematically lower in L1495B, L1521B, and L1521E than in the other dark cores (Hirota et al. 2001, 2003). These features suggest

that L1495B, L1521B, and L1521E would be in the early stage of dynamical and chemical evolution, and the degree of depletion of molecules is possibly lower than in other evolved cores (Tafalla & Santiago 2004).

Although detailed studies on carbon-chain-producing regions are important for understanding of chemical and physical evolution of dense cores, only four carbon-chain-producing regions were identified in Taurus Molecular Cloud. In order to search for carbon-chain-producing regions outside the Taurus Molecular Cloud, we carried out a survey of CCS, HC<sub>3</sub>N, and HC<sub>5</sub>N toward 31 dark cloud cores. As a result, we detected a possible candidate for another carbon-chain-producing region L492 in the Aquila Rift (Hirota et al. in preparation). L492 is one of the prestellar cores identified as a strong infalling candidate (Lee et al. 2001), and it is observed with the dust continuum emission as well as the N<sub>2</sub>D<sup>+</sup> and N<sub>2</sub>H<sup>+</sup> lines (Crapsi et al. 2005). In this paper, we report on the results of extensive molecular line observations of L492.

## 2. Observations

We carried out molecular line observations of L492 with the 45 m radio telescope at Nobeyama Radio Observatory (NRO)<sup>1</sup> in February 2003 and March 2004. The observed lines are summarized in Table 1.

We used cooled HEMT receivers for the lines in the 22-23 GHz band, SIS mixer receivers for the lines in the 45-48 GHz and 72-96 GHz bands, the SIS 25-beam array receiver system (BEARS) for the <sup>13</sup>CO and C<sup>18</sup>O lines in the 109-110 GHz band. The main-beam efficiencies ( $\eta_{mb}$ ) were 0.8, 0.7, 0.5, and 0.5 for the 22-23 GHz, 45-49 GHz, 72-96 GHz, and 109-110 GHz bands, respectively. The beam sizes were 73'', 36'', 20'', and 16'' for the 22-23 GHz, 45-49 GHz, 72-96 GHz, and 109-110 GHz bands, respectively. Acousto-optical radio spectrometers with the frequency resolution of 37 kHz were used for the backend except for the <sup>13</sup>CO and C<sup>18</sup>O observations, in which autocorrelators with the frequency resolution of 31.25 kHz were used.

We took the reference position of L492 to be  $\alpha_{2000} = 18^h 15^m 46^s .1$ ,  $\delta_{2000} = -03^\circ 46' 13''$  (Lee et al. 2001; Crapsi et al. 2005). Observations in the 22-23 GHz and 45-49 GHz bands were performed in the position-switching mode. The off position was taken to be 10' away from the source position, which is outside the core of L492 with the radius of 3.2' (Lee & Myers

---

<sup>1</sup>Nobeyama Radio Observatory is a branch of the National Astronomical Observatory of Japan, an interuniversity research institute operated by the Ministry of Education, Science, Sports and Culture of Japan

1999). Observations in the 72-96 GHz and 109-110 GHz bands were performed in the frequency switching mode with the frequency offset was set to be 7.685 MHz. The grid spacing in the mapping observations was taken to be 40-80'', 40'', and 20'' for the 22-23 GHz, 45-49 GHz, and 72-96 GHz bands, respectively, as shown in Figure 1. Since the beam separation of the BEARS is 41.1'', the grid spacing of the  $^{13}\text{CO}$  and  $\text{C}^{18}\text{O}$  maps were taken to be 20.55''. Note that we did not carry out the Niquist sampling because of limited observing time. Pointing was checked by observing a nearby SiO maser source, R-Aql, every 1-2 hours, and the pointing accuracy was estimated to be better than 5''. The antenna temperature was calibrated by a usual chopper-wheel method.

### 3. Results

#### 3.1. Molecular Distributions and Velocity Structure

Figure 1 shows the integrated intensity maps, and Figures 2-5 show an example of the observed spectrum for each molecule. We only show the maps of the lines marked in Table 1. The molecular gas is distributed along the north-south ridge traced by the  $^{13}\text{CO}$  and  $\text{C}^{18}\text{O}$  lines, and the dense core of L492 traced by other lines is located at the southern edge of the ridge. Most of the maps show quite similar structure with a single peak and a simple elliptical shape with the average diameter of 100'', corresponding to 0.1 pc at the distance of 200 pc (Lee & Myers 1999). Although the peak positions are different from each other, this is partly due to the different beam size and grid spacing. The single peak distribution of the  $\text{C}^{34}\text{S}$  and CCS in L492 clearly contrasts with the double peak distribution in L1498 and L1544 (Kuiper et al. 1996; Ohashi et al. 1999; Tafalla et al. 2002, 2004), and is rather similar to the distribution in the carbon-chain-producing regions such as L1495B, L1521B, and L1521E (Hirota et al. 2002, 2004). The peak position of the  $\text{N}_2\text{H}^+$  map is 20'' south of those of the dust continuum,  $\text{N}_2\text{D}^+$ , and  $\text{N}_2\text{H}^+$  maps reported by Crapsi et al. (2005), probably due to insufficient spatial resolution or coarse grid spacing.

On the other hand, we found a marginal double peak structure in the maps of the  $J=1-0$  line of  $\text{H}^{13}\text{CO}^+$  and the  $7_6-6_5$  line of CCS, although the northern peak has the statistical significance of only  $2\sigma$  level. Because the optical depth of the  $J=1-0$  line of  $\text{H}^{13}\text{CO}^+$  and the  $7_6-6_5$  line of CCS are 0.82 and 0.54, respectively, as discussed later, they would not be suffered from self-absorption. A possible explanation is depletion of  $\text{H}^{13}\text{CO}^+$  and CCS in the central part of the core. Note that the double peak structure is not evident in the CCS  $4_3-3_2$  map as mentioned above. Since the critical density for the  $7_6-6_5$  line is higher than that of the  $4_3-3_2$  line, we could detect the depletion of CCS only with the  $7_6-6_5$  line. If the double peak structure is real, the depletion of molecules would have just started at the central part

of L492, which can be seen only in the  $7_6-6_5$  line of CCS and the  $J=1-0$  line of  $\text{H}^{13}\text{CO}^+$ . Further high resolution observations would be necessary to confirm this.

It is interesting to compare the deuterium fractionation ratio within the dense core, because the deuterium fractionation ratio reflects chemical evolutionary stage and degree of depletion (Caselli et al. 2002b; Hirota et al. 2001, 2003). Figure 6 shows the integrated intensity ratios of  $\text{DCO}^+/\text{H}^{13}\text{CO}^+$  and  $\text{DNC}/\text{HN}^{13}\text{C}$  as a function of the distance from the dust continuum peak. Because these lines are optically thin as discussed later, the integrated intensity ratios approximately represent the abundance ratios. The maximum  $\text{DCO}^+/\text{H}^{13}\text{CO}^+$  and  $\text{DNC}/\text{HN}^{13}\text{C}$  ratios are 1.6 and 2.2, respectively, and their positions are offset from the  $\text{DCO}^+$  and  $\text{DNC}$  peaks and also from the dust continuum peak. The deuterium fractionation ratios are not significantly enhanced in the central part of the core. We might be able to see an only slight increase in the  $\text{DCO}^+/\text{H}^{13}\text{CO}^+$  ratio within the inner  $40''$  area. However, this is not so clear as in the case of L1544 (Caselli et al. 2002b). As for the  $\text{DNC}/\text{HN}^{13}\text{C}$  ratio, such an enhancement is not seen, being consistent with other cores (Hirota et al. 2003).

We also investigate velocity structure of the core using the CCS ( $7_6-6_5$ ) line, because this line has no hyperfine splitting and was observed with a relatively high velocity resolution ( $0.136 \text{ km s}^{-1}$ ). Figures 7 and 8 show the channel maps and position-velocity diagrams of the CCS( $7_6-6_5$ ) line, respectively. We found a global velocity gradient of  $3 \text{ km s}^{-1} \text{ pc}^{-1}$  in the east-west direction across the core. On the other hand, we could not find other significant change in the linewidth (e.g. Crapsi et al. 2005). According to Lee et al. (2001), the optically thick line, CS( $J=2-1$ ), toward L492 has the asymmetric line profile due to an infalling motion. However, either double peak or asymmetric line profiles are not detected in our observations because we observed only optically thin lines.

### 3.2. Abundances for Individual Molecules

In order to evaluate abundances of the observed molecules, line parameters for all the observed lines were determined by the Gaussian fit, as summarized in Table 1. We ignored unresolved hyperfine structures of the  $\text{NH}_3$  and  $\text{HC}_3\text{N}$  lines, and hence, their linewidths are shown to be broader than the others. The parameters at the ( $0''$ ,  $0''$ ) position for  $\text{NH}_3$  and  $\text{HC}_7\text{N}$  (22-23 GHz band), the ( $40''$ ,  $0''$ ) position for other carbon-chain molecules (22-23 GHz, 45-49 GHz and 81-96 GHz bands), and the ( $20''$ ,  $20''$ ) position for the rest (72-93 GHz and 109-110 GHz bands) are listed in Table 1. These positions correspond to the peak positions of the integrated intensity map for each molecule. Using these line parameters, we calculated the column densities of the observed molecules by the consistent way employed in previous

works (e.g. Suzuki et al. 1992; Hirota et al. 1998, 2001, 2002, 2004) in order to compare the present results with those for L1495B, L1521B, L1521E, and TMC-1. The methods are briefly described below, and the results are summarized in Tables 2 and 3. The references for collision rates and dipole moments are also summarized in Tables 2 and 3. In the analysis, the kinetic temperature in L492 is assumed to be 10 K, which was derived from the  $\text{NH}_3$  lines in the present study. Because we observed molecular lines with the different grid spacing depending on the beam size, we can not compare the line parameters and column densities of all the observed molecules at the same position. Therefore, we list the line parameters and molecular column densities at the above positions. Although the peak positions are different from each other, this is partly due to the different beam size and grid spacing. Therefore, the column densities for the positions listed in Tables 2 and 3 would be those for the same volume of gas. According to our maps shown in Figure 1, the difference in the integrated intensities due to the position difference is less than 20%, and hence, the uncertainty in the column densities due to the position difference is estimated to be 20%.

### 3.2.1. $\text{C}^{34}\text{S}$

We derived the column density of  $\text{C}^{34}\text{S}$  and the  $\text{H}_2$  density using the large velocity gradient (LVG) model (Goldreich & Kwan 1974). The method is the same as that adopted in Hirota et al. (1998). We ignored the difference in the beam sizes between the  $J=1-0$  and  $2-1$  lines in the analysis. Because the core size of L492 ( $100''$ ) is sufficiently larger than the beam sizes for the  $J=1-0$  ( $36''$ ) and  $J=2-1$  line ( $20''$ ), this approximation does not seriously affect the results (e.g. Hirota et al. 1998). The  $\text{H}_2$  density is derived to be  $9.0 \times 10^4 \text{ cm}^{-3}$ .

### 3.2.2. $\text{CCS}$

We derived the column density of CCS and the  $\text{H}_2$  density using the LVG model. Because the beam size of the  $J_N=2_1-1_0$  lines are as large as the core size, beam dilution effect would be significant, and hence, we only used the results of the  $J_N=4_3-3_2$  and  $J_N=7_6-6_5$  lines. For these lines, we ignored the difference in the beam sizes of the two transitions, as in the case of the  $\text{C}^{34}\text{S}$  analysis. The  $\text{H}_2$  density is derived to be  $6.8 \times 10^4 \text{ cm}^{-3}$ .

For comparison, we carried out LTE analysis assuming the excitation temperature of 5 K (Suzuki et al. 1992; Hirota et al. 1998, 2002, 2004). In this case, column density of CCS is three times larger than that derived from the LVG analysis. Therefore, the column densities of CCS for other cores obtained by the LTE analysis, in which the excitation temperature

is fixed to 5 K, would be overestimated. In this paper, the LTE value is employed for consistency with previous results.

### 3.2.3. $DCO^+$ , $DNC$ , $H^{13}CO^+$ , $HN^{13}C$

We derived the column densities of  $DCO^+$ ,  $DNC$ ,  $H^{13}CO^+$ , and  $HN^{13}C$  by the LVG calculations. The method is described in Hirota et al. (2001). Because we did not carry out multi-transition observations for these molecules, we assumed the  $H_2$  density to be  $9.0 \times 10^4 \text{ cm}^{-3}$ , which is derived from the  $C^{34}S$  data. If we assume the  $H_2$  density to be  $2.0 \times 10^5 \text{ cm}^{-3}$  (Crapsi et al. 2005), the column densities of  $DCO^+$  and  $H^{13}CO^+$  decrease by 10-25%, while those of  $DNC$  and  $HN^{13}C$  decrease by a factor of 2. In both case, the  $DCO^+/H^{13}CO^+$  and  $DNC/HN^{13}C$  ratios change by less than 10%.

### 3.2.4. $^{13}CO$ , $C^{18}O$

The column densities of  $^{13}CO$  and  $C^{18}O$  were derived by assuming the  $^{13}CO/C^{18}O$  ratio of the local ISM value, 7.3 (Wilson & Rood 1994), and the common excitation temperature. The excitation temperature was determined to be 8.3 K.

### 3.2.5. $HC_3N$

At first, we carried out the LVG analysis using the  $J=5-4$  and  $9-8$  lines to derive the column density of  $HC_3N$  and the  $H_2$  density. However, the fitting did not converge probably because of the large optical depth of the  $J=5-4$  line. Because the satellite hyperfine component of the  $J=5-4$  line is clearly detected as shown in Figure 3, we can determine the optical depth and the excitation temperature of the  $J=5-4$  line of  $HC_3N$ . The total optical depth and the excitation temperature were calculated to be 8.8 and 6.4 K, respectively. The excitation temperature determined here is consistent with that employed by Suzuki et al. (1992), 6.5 K. Then we determined the column density of  $HC_3N$  from the total optical depth assuming the LTE condition with the excitation temperature of 6.4 K.

### 3.2.6. $C_3S$ , $HC_5N$ , $HC_7N$

For  $C_3S$ ,  $HC_5N$ , and  $HC_7N$ , we determined their column densities by the consistent way adopted in the previous literatures (e.g. Hirota et al. 2002, 2004; Cernicharo et al. 1986). We assumed that the excitation temperatures of 5.5 K for  $C_3S$ , 6.5 K for  $HC_5N$ , and 10.0 K for  $HC_7N$ .

### 3.2.7. $N_2H^+$

Since all the hyperfine components of the  $N_2H^+$  line are detected as shown in Figure 4, we were able to determine the optical depth and the excitation temperature of  $N_2H^+$  to be 6.1 and 4.9 K, respectively. The excitation temperature determined here is consistent with those reported by Caselli et al. (2002a), 5 K. Then we derived the column density of  $N_2H^+$  assuming the LTE condition with the excitation temperature of 4.9 K.

### 3.2.8. $NH_3$

Using the intensity ratios of hyperfine components of the (1,1) lines, we derived the excitation temperature to be 4.1 K. In addition, we determined the rotation temperature of the para  $NH_3$  to be  $9.5^{+1.7}_{-1.0}$  K by the methods described in Ho & Townes (1983). Thus, we calculated the column density of  $NH_3$  assuming the LTE condition with the rotation temperature of 10 K and the ortho-to-para ratio of 1.

## 4. Discussions

The column densities of the observed molecules are summarized in Table 4. For comparison, the corresponding column densities in the carbon-chain-producing regions are also listed in Table 4. The column densities of the carbon-chain molecules in L492 are significantly higher than those in typical dark cloud cores (Suzuki et al. 1992) and are comparable to those in the carbon-chain-producing regions such as L1495B, L1521B, L1521E, and TMC-1. Since the carbon-chain-producing regions have so far been recognized in the Taurus Molecular Cloud, L492 is the first dark cloud core with extremely high abundances of carbon-chain-molecules that is found outside the Taurus Molecular Cloud. On the other hand, the column densities of  $NH_3$  and  $N_2H^+$  in L492 are higher than those in the carbon-chain-producing regions, and are comparable to those in typical dark cloud cores (Benson & Myers 1989; Suzuki



et al. 1992; Caselli et al. 2002a). We stress that the column densities in L492 are almost comparable to those of TMC-1 for most of the observed molecules, except for the slightly high column density of  $\text{NH}_3$  and the low column densities of sulfur-bearing carbon-chain molecules and  $\text{HC}_7\text{N}$ . Thus the chemical composition in L492 is close to that of TMC-1.

In order to discuss chemical evolutionary stages of L492 and other starless cores, we summarize the selected molecular abundance ratios which are thought to be used as a chemical clock, as shown in Table 5. The most popular indicator is the  $\text{NH}_3/\text{CCS}$  ratio (Suzuki et al. 1992). The  $\text{NH}_3/\text{CCS}$  ratio of 6.5 in L492 is intermediate between those of carbon-chain-producing regions (2.6-3.8) and evolved prestellar core such as L1498 and L1544 (15-25). For consistency, we employed the  $\text{NH}_3/\text{CCS}$  ratios in L1498 and L1544 reported by Suzuki et al. (1992). Uncertainties in the  $\text{NH}_3/\text{CCS}$  ratios are quite large due to difference in telescope beam sizes, observed positions, and methods of data analysis. In fact, different values are reported by Aikawa et al. (2005) (14-25 and 9.0 for L1498 and L1544, respectively). If we use the result of the LVG calculations for the column density of CCS, the  $\text{NH}_3/\text{CCS}$  ratio in L492 is 21, which is larger by a factor of 3 than that of the LTE value. Even such uncertainties are considered, we can say that the  $\text{NH}_3/\text{CCS}$  ratio in L492 is intermediate or close to those of L1498 and L1544 rather than those in carbon-chain-producing regions.

Another good indicator for chemical evolutionary stage is a deuterium fractionation ratio. Because deuterium fractionation proceeds through the exothermic isotope exchange reaction of  $\text{H}_3^+$  and HD in the gas-phase, the  $\text{H}_2\text{D}^+/\text{H}_3^+$  ratio gradually increase with time (e.g. Roberts & Millar 2000; Turner 2001; Hirota et al. 2001; Saito et al. 2002). In addition, depletion of molecules make the life time of  $\text{H}_2\text{D}^+$  longer, resulting in a high deuterium fractionation ratio of  $\text{H}_2\text{D}^+/\text{H}_3^+$ . Consequently, a deuterium fractionation ratio is thought to be enhanced in evolved cores (e.g. Roberts & Millar 2000; Turner 2001; Hirota et al. 2001; Saito et al. 2002). The deuterium fractionation ratio,  $\text{DNC}/\text{HN}^{13}\text{C}$ , of 1.27 in L492 is comparable to those of the carbon-chain-producing regions (0.66-1.25), and is smaller than those in L1498 (1.91) and L1544 (3.0). The  $\text{DCO}^+/\text{H}^{13}\text{CO}^+$  ratio of 0.80 is also comparable to those of the carbon-chain-producing regions (0.63-1.10) and smaller than those in L1498 (2.7) and L1544 (3.1-9.2). The lower  $\text{DCO}^+/\text{H}^{13}\text{CO}^+$  ratio in L492 suggests that molecular depletion is not very significant in comparison with L1544 (Caselli et al. 2002b). The  $\text{N}_2\text{D}^+/\text{N}_2\text{H}^+$  ratio of 0.05 in L492 is comparable to that in L1498 (0.04), while it is lower than in L1544 (0.23) (Crapsi et al. 2005). These results suggest that chemical evolutionary stage of L492 would be younger than those of L1498 and L1544, and molecules would be less depleted in L492 than in L1498 and L1544.

## 5. Evolutionary Scenario of L492 and Other Cores

Recently, discussions considering both dynamical and chemical evolution of dense cores have been reported (Lee et al. 2003; Aikawa et al. 2005; Crapsi et al. 2005; Shirley et al. 2005). For comparison, we summarize the evolutionary stages of L492 and other starless cores on the basis of signature of dynamical collapse, degree of depletion, and molecular abundance ratios, as shown in Table 6. As already reported, L492 is in the dynamically collapsing phase as well as L1498 and L1544 (Ohashi et al. 1999; Lee et al. 2001; Crapsi et al. 2005), while L1521B, L1521E, and TMC-1 are not (Lee et al. 1999; Hirota et al. 2002, 2004). Therefore, L492 can be regarded as a dynamically evolved core. Crapsi et al. (2005) recently reported that a degree of depletion of CO in L492 is comparable to that in L1498 and is lower than in L1544. On the other hand, the depletion of CO would not occur significantly in the carbon-chain-producing regions such as L1521E (Tafalla & Santiago 2004). Our results on the CS and CCS distributions suggest that depletion of these molecules seems to be less significant than in L1498 and L1544 (Tafalla et al. 2002, 2004). Therefore, a degree of depletion of molecules in L492 is intermediate between chemically young cores (L1521E) and evolved cores (L1498 and L1544). The deuterium fractionation ratios of DNC/HN<sup>13</sup>C and DCO<sup>+</sup>/H<sup>13</sup>CO<sup>+</sup> in L492 are lower than those in L1498 and L1544, and are comparable to those in carbon-chain-producing regions. This means that L492 is chemically younger than L1498 and L1544. Finally, the NH<sub>3</sub>/CCS ratio in L492 is larger than those in carbon-chain-producing regions and is smaller than in L1498 and L1544, suggesting that L492 is more evolved than in carbon-chain-producing regions but is younger than L1498 and L1544.

Considering these results, we conclude that the evolutionary stage of L492 is intermediate between the carbon-chain-producing regions (L1495B, L1521B, L1521E, and TMC-1) and evolved prestellar cores (L1498 and L1544). We propose the following scenario for chemical and dynamical evolution. At the initial state of dense cores before protostellar collapse, such as L1495B, L1521B, L1521E, and TMC-1, abundances of carbon-chain molecules are extremely high because of high abundance of the neutral carbon atom (Suzuki et al. 1992). On the other hand, NH<sub>3</sub> and N<sub>2</sub>H<sup>+</sup> are not yet abundant because they are produced by slow chemical reactions (Suzuki et al. 1992; Bergin & Langer 1997; Aikawa et al. 2005). In addition, the deuterium fractionation in these cores are not enhanced because of the low H<sub>2</sub>D<sup>+</sup>/H<sub>3</sub><sup>+</sup> ratio at the earliest stage of chemical evolution, and also because of a low degree of depletion of CO, CS, CCS, and other molecules (Roberts & Millar 2000; Turner 2001; Hirota et al. 2001; Saito et al. 2002). As a core evolves, abundances of carbon-chain molecules are still high while those of NH<sub>3</sub> and N<sub>2</sub>H<sup>+</sup> increase by the gas-phase reactions (Suzuki et al. 1992; Bergin & Langer 1997), and hence, the NH<sub>3</sub>/CCS ratio increases with time. This would be the stage of L492. For L492, depletion of CS and CCS is less significant than L1498 and L1544, while the CO molecules start to deplete (Crapsi et al. 2005). Depletion of

molecules would be just started in the central part of L492, if the double peak structure of the  $\text{H}^{13}\text{CO}^+$  ( $J=1-0$ ) and CCS ( $7_6-6_5$ ) maps reflect real abundance variation. At the earliest phase of molecular depletion such as in L492, the deuterium fractionation is not significantly affected by the depletion. In this phase, protostellar collapse has already started (Lee et al. 2001). As a core further evolves, the abundances of carbon-chain molecules decrease due to gas-phase reactions and freeze-out of molecules onto grains while abundances of  $\text{NH}_3$  and  $\text{N}_2\text{H}^+$  increase significantly (Suzuki et al. 1992; Bergin & Langer 1997). This results in high  $\text{NH}_3/\text{CCS}$  ratio. The L1498 core would be just around this stage. The increase in the deuterium fractionation seems to be different from molecule to molecule. The  $\text{N}_2\text{D}^+/\text{N}_2\text{H}^+$  ratio increases more slowly than the  $\text{DCO}^+/\text{HCO}^+$  and  $\text{DNC}/\text{HN}^{13}\text{C}$  ratios. At the most evolved phase like L1544, depletion of molecule is significant, and the deuterium fractionation ratio increases drastically.

It is also likely that timescales of gas-phase chemical evolution, freeze-out of molecules onto grains, and dynamical collapse are different from region to region (e.g. Taurus and Aquila Rift). For example, Lee et al. (2003) and Shirley et al. (2005) classified three types of prestellar cores; chemically evolved and dynamically young cores (L1512, L1498), chemically evolved and dynamically evolved cores (L1544), and chemically young and dynamically evolved cores (L1689B). Lee et al. (2003) suggest that L1689B, which is in the Ophiuchus region, has the different environment from those of L1512 and L1544 in the Taurus region. It should be noted that L492 is also a chemically young and dynamically evolved core outside the Taurus region. In order to understand this regional difference, further systematic observational studies and theoretical modeling would be needed.

We are grateful to the staff of Nobeyama Radio Observatory for their assistance in observations. TH thanks to the Inoue Foundation for Science (Research Aid of Inoue Foundation for Science) for the financial support. This study is partly supported by Grant-in-Aid from Ministry of Education, Science, Sports and Culture of Japan (14204013 and 15071201).

## REFERENCES

- Aikawa, Y., Herbst, E., Roberts, H., and Caselli, P. 2005, *ApJ*, 620, 330
- Alexander, A. J., Kroto, H. W., & Walton, D. R. M. 1976, *J. Mol. Spectrosc.*, 62, 175
- Benson, P. J., & Myers, P. C. 1989, *ApJS*, 71, 89
- Bergin, E. A. & Langer, W. D. 1997, *ApJ*, 486, 316

- Blackman, G. L., Brown, R. D., Godfrey, P. D., & Gunn, H. I. 1976, *Nature*, 261, 395
- Botschwina, P., Horn, M., Markey, K., & Oswald, R. 1997, *Mol. Phys.* 92, 381
- Butner, H. M., Lada, E. A., & Loren, R. B. 1995, *ApJ*, 448, 207
- Caselli, P., Benson, P. J., Myers, P. C., & Tafalla, M. 2002a, *ApJ*, 572, 238
- Caselli, P., Walmsley, C. M., Tafalla, M., Dore, L., & Myers, P. C. 1999, *ApJ*, 523, L165
- Caselli, P., Walmsley, C. M., Zucconi, A., Tafalla, M., Dore, L., & Myers, P. C. 2002b, *ApJ*, 565, 344
- Cernicharo, J., Bachiller, R., & Duvert, G. 1986, *A&A*, 160, 181
- Cohen, E. A., & Poynter, R. L. 1974, *J. Mol. Spectrosc.*, 53, 131
- Crapsi, A., Caselli, P., Walmsley, C. M., Myers, P. C., Tafalla, M., Lee, C. W., & Bourke, T. L. 2005, *ApJ*, 619, 379
- Goldreich, P. & Kwan, J. 1974, *ApJ*, 189, 441
- Goorvitch, D. 1994, *ApJS*, 95, 535
- Green, S., & Chapman, S. 1978, *ApJS*, 37, 169
- Green, S., & Thaddeus, P. 1974, *ApJ*, 191, 653
- Haese, N. N., & Woods, R. C. 1979, *Chem. Phys. Lett.*, 61, 396
- Havenith, M., Zwart, E., Meerts, W. L., ter Meulen, J. J. 1990, *J. Chem. Phys.*, 93, 8446
- Hirahara, Y., et al. 1992, *ApJ*, 394, 539
- Hirahara, Y., et al. 1995, *PASJ*, 47, 845
- Hirota, T., Yamamoto, S., Mikami, H., & Ohishi, M. 1998, *ApJ*, 503, 717
- Hirota, T., Ikeda, M., & Yamamoto, S. 2001, *ApJ*, 547, 814
- Hirota, T., Ikeda, M., & Yamamoto, S. 2003, *ApJ*, 594, 859
- Hirota, T., Ito, T., & Yamamoto, S. 2002, *ApJ*, 565, 359
- Hirota, T., Maezawa, H., & Yamamoto, S. 2004, *ApJ*, 617, 399
- Ho, P. T. P. & Townes, C. H. 1983, *ARA&A*, 21, 239

- Kuiper, T. B. H., Langer, W. D., & Velusamy, T. 1996, *ApJ*, 468, 761
- Lafferty, W. J., & Lovas, F. J. 1978, *J. Phys. Chem. Ref. Data*, 7, 441
- Lee, C. W. & Myers, P. C. 1999, *ApJS*, 123, 233
- Lee, C. W., Myers, P. C., & Tafalla, M. 1999, *ApJ*, 526, 788
- Lee, C. W., Myers, P. C., & Tafalla, M. 2001, *ApJS*, 136, 703
- Lee, J.-E., Evans N. J., II, Shirley, Y. L., and Tatematsu, K. 2003, *ApJ*, 583, 789
- Monteiro, T. S. 1985, *MNRAS*, 214, 419
- Murakami, A. 1990, *ApJ*, 357, 288
- Myers, P. C., Mardones, D., Tafalla, M., Williams, J. P., & Wilner, D. J. 1996, *ApJ*, 465, L133
- Myers, P. C., Linke, R. A., & Benson, P. J. 1983, *ApJ*, 264, 517
- Ohashi, N., Lee, S. W., Wilner, D. J., & Hayashi, M. 1999, *ApJ*, 518, L41
- Pratap, P., Dickens, J. E., Snell, R. L., Miralles, M. P., Bergin, E. A., Irvine, W. M., & Schloerb, F. P. 1997, *ApJ*, 486, 862
- Roberts, H. & Millar, T. J. 2000, *A&A*, 361, 388
- Saito, S., Aikawa, Y., Herbst, E., Ohishi, M., Hirota, T., Yamamoto, S., & Kaifu, N. 2002, *ApJ*, 569, 836
- Shirley, Y. L., Nordhaus, M. K., Grcevich, J. M., Evans N. J., II, Rawlings, J. M. C., and Tatematsu, K. 2005, *ApJ*, 632, 982
- Suzuki, H., Yamamoto, S., Ohishi, M., Kaifu, N., Ishikawa, S., Hirahara, Y., & Takano, S. 1992, *ApJ*, 392, 551
- Tafalla, M., Myers, P. C., Caselli, P., & Walmsley, C. M. 2004, *A&A*, 416, 191
- Tafalla, M., Myers, P. C., Caselli, P., Walmsley, C. M., & Comito, C. 2002, *ApJ*, 569, 815
- Tafalla, M. & Santiago, J. 2004, *A&A*, 414, L53
- Turner, B. E. 2001, *ApJS*, 136, 579
- Ungerechts, H., Walmsley, C. M., & Winnewisser, G. 1980, *A&A*, 88, 259

- Wilson, T. L. & Rood, R. T. 1994, *ARA&A*, 32, 191
- Winnewisser, G. & Cook, R. L. 1968, *J. Mol. Spectrosc.*, 28, 266
- Wolkovitch, D., Langer, W. D., Goldsmith, P. F., & Heyer, M. 1997, *ApJ*, 477, 241
- Yamamoto, S., Shuji, S., Kawaguchi, S., Chikada, Y., Suzuki H., Kaifu, N., Ishikawa, S., & Ohishi, M. 1990, *ApJ*, 361, 318

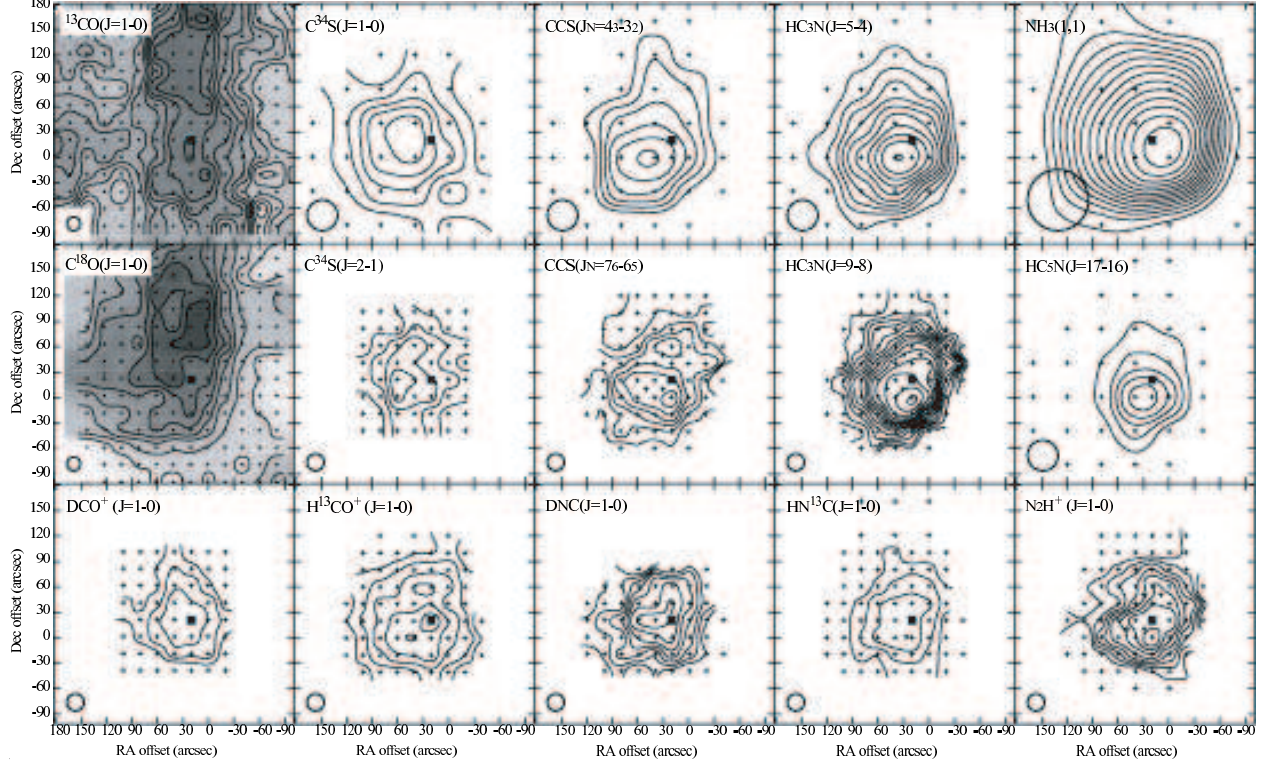


Fig. 1.— Integrated intensity maps of molecular lines in L492. The velocity range of integration (in  $\text{km s}^{-1}$ ), the interval of the contours ( $2\sigma$ , in  $\text{K km s}^{-1}$ ) and the lowest contour ( $3\sigma$ , in  $\text{K km s}^{-1}$ ) are (7.0-9.0, 0.24, 0.36) for  $^{13}\text{CO}(J=1-0)$ , (7.0-8.5, 0.070, 0.105) for  $\text{C}^{34}\text{S}(J=1-0)$ , (7.2-8.3, 0.100, 0.150) for  $\text{CCS}(4_3-3_2)$ , (7.0-8.5, 0.200, 0.300) for  $\text{HC}_3\text{N}(J=5-4)$ , (7.2-8.6, 0.100, 0.150) for  $\text{NH}_3(1,1)$ , (7.2-8.8, 0.150, 0.225) for  $\text{C}^{18}\text{O}(J=1-0)$ , (7.3-8.2, 0.050, 0.075) for  $\text{C}^{34}\text{S}(J=2-1)$ , (7.2-8.3, 0.060, 0.090) for  $\text{CCS}(7_6-6_5)$ , (7.2-8.3, 0.060, 0.090) for  $\text{HC}_3\text{N}(J=9-8)$ , (7.3-8.3, 0.100, 0.150) for  $\text{HC}_5\text{N}(J=17-16)$ , (7.2-8.3, 0.110, 0.165) for  $\text{DCO}^+(J=1-0)$ , (7.2-8.5, 0.080, 0.120) for  $\text{H}^{13}\text{CO}^+(J=1-0)$ , (7.0-8.5, 0.070, 0.105) for  $\text{DNC}(J=1-0)$ , (7.0-8.5, 0.080, 0.120) for  $\text{HN}^{13}\text{C}(J=1-0)$ , and (−0.6-15.2, 0.200, 0.300) for  $\text{N}_2\text{H}^+(J=1-0, \text{total})$ . For the  $\text{NH}_3(1,1)$  line, the integrated intensity is the sum of all 5 components (see text and Table 1). For the  $\text{N}_2\text{H}^+(J=1-0)$  line, the velocity range of integration is for the  $F_1, F=2,3-1,2$  component. The beam size (HPBW) is shown in the lower left of each map. The peak position of the dust continuum emission (Crapsi et al. 2005) is indicated by a filled square, and observed positions are indicated by small crosses. Gray scale maps are superposed to the  $^{13}\text{CO}(J=1-0)$  and  $\text{C}^{18}\text{O}(J=1-0)$  maps to clarify their complex structures.

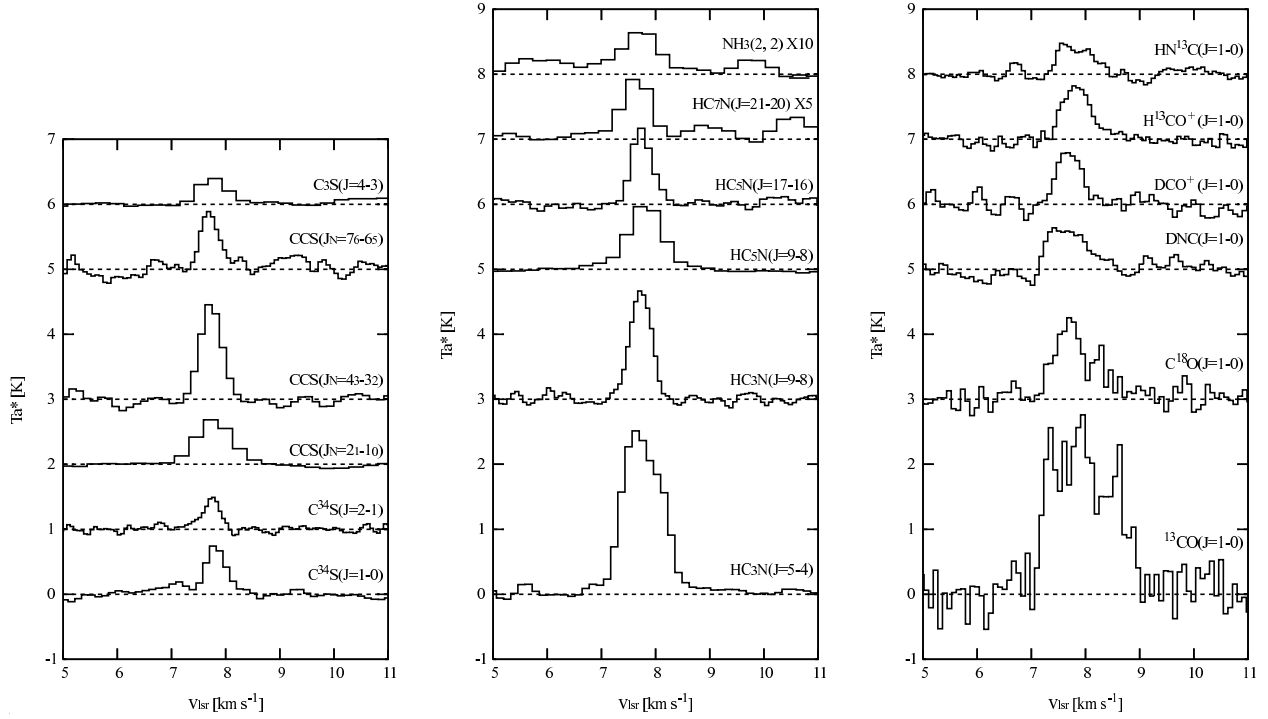


Fig. 2.— Examples of the observed spectral lines. *Left:* Spectra of sulphur-bearing molecules. They are observed toward the (40'', 0'') position of L492. *Middle:* Spectra of cyanopolynes and  $NH_3$ . They are observed toward the (40'', 0'') position of L492, except for  $NH_3(2,2)$  and  $HC_7N(J=21-20)$ , which are observed at the (0'', 0'') position. *Right:* Spectra of deuterated molecules and CO isotopes. They are observed toward the (20'', 20'') position of L492.



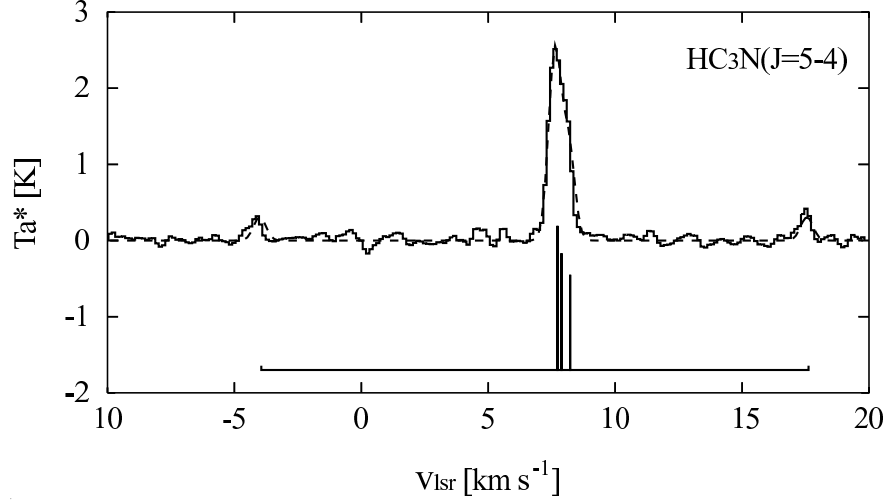


Fig. 3.— A spectrum of  $\text{HC}_3\text{N}(J=5-4)$  at the  $(40'', 0'')$  position of L492. A dashed line represents the best fit model. The expected hyperfine pattern of the  $\text{HC}_3\text{N}$  line is indicated in the bottom of the figure.

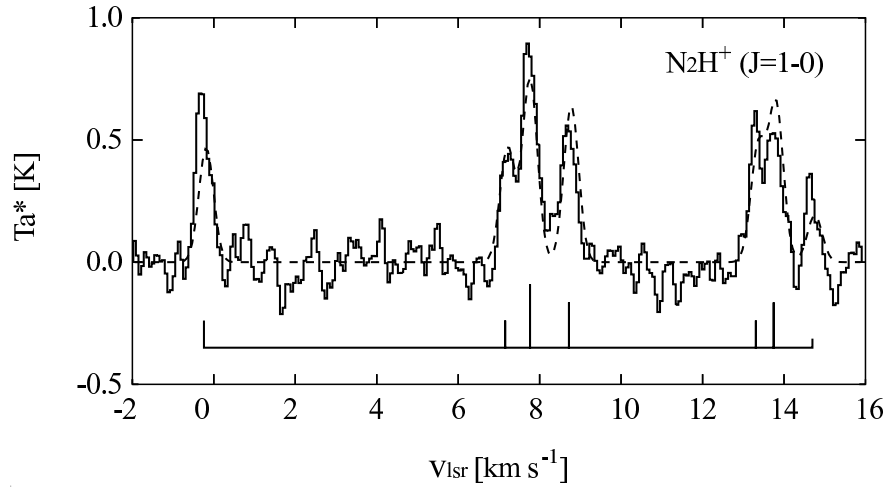


Fig. 4.— A spectrum of  $\text{N}_2\text{H}^+(J=1-0)$  at the  $(20'', 20'')$  position of L492. A dashed line represents the best fit model. The expected hyperfine pattern of the  $\text{N}_2\text{H}^+$  line is indicated in the bottom of the figure.

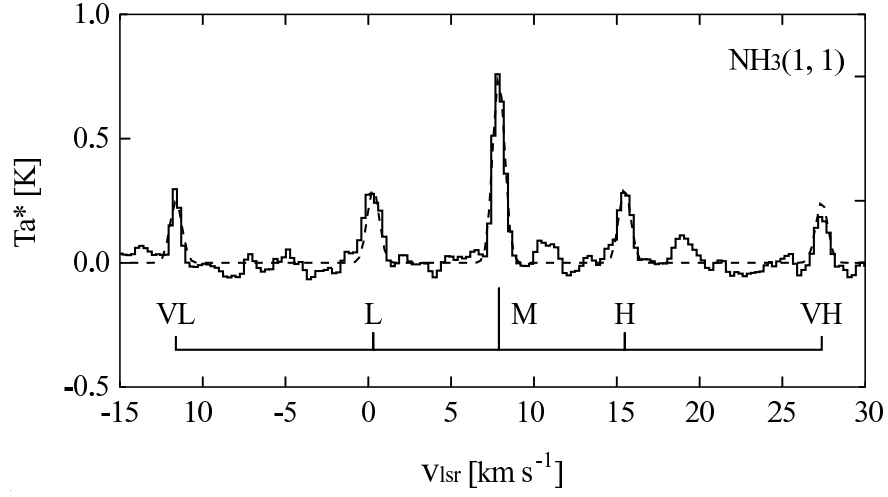


Fig. 5.— A spectrum of  $\text{NH}_3(J, K=1, 1)$  at the  $(0'', 0'')$  position of L492. A dashed line represents the best fit model. The expected hyperfine pattern of the  $\text{NH}_3$  line are indicated in the bottom of the figure. Groups of blended hyperfine components are labeled as adopted by Ungerechts et al. (1980).

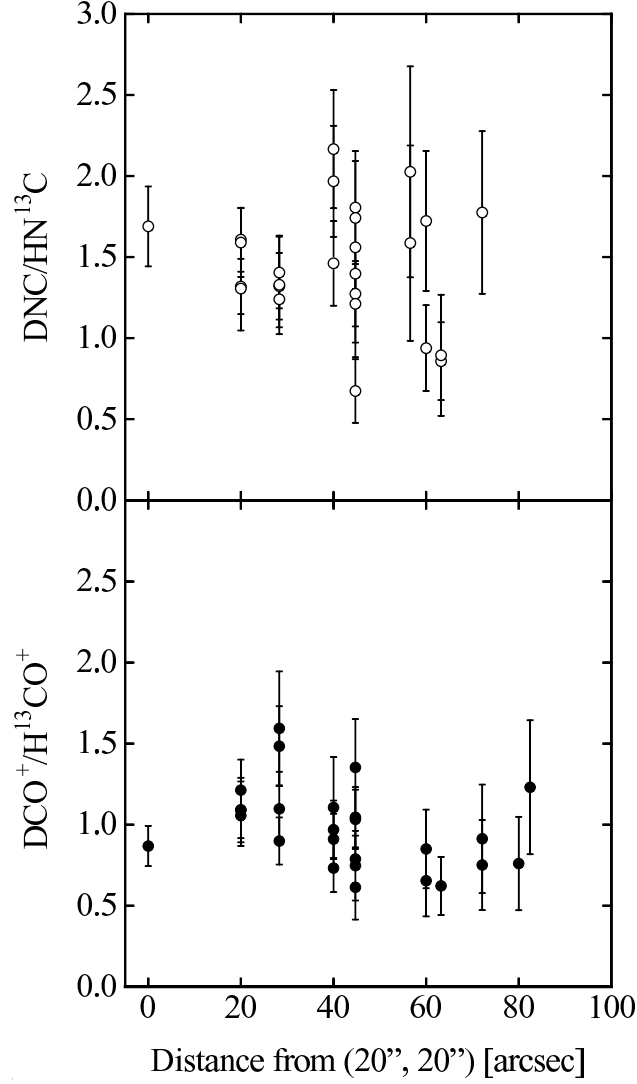


Fig. 6.— Integrated intensity ratio of deuterated molecules as a function of the distance from the dust continuum peak. *Top*:  $\text{DNC}^+/\text{HN}^{13}\text{C}$  ratio. *Bottom*:  $\text{DCO}^+/\text{H}^{13}\text{CO}^+$  ratio. Errors are estimated from the rms noise of each spectrum ( $2\sigma$ ). Because these lines are optically thin, the integrated intensity ratios approximately represent the deuterium fractionation ratios as a function of the distance from the dust continuum peak (see text).

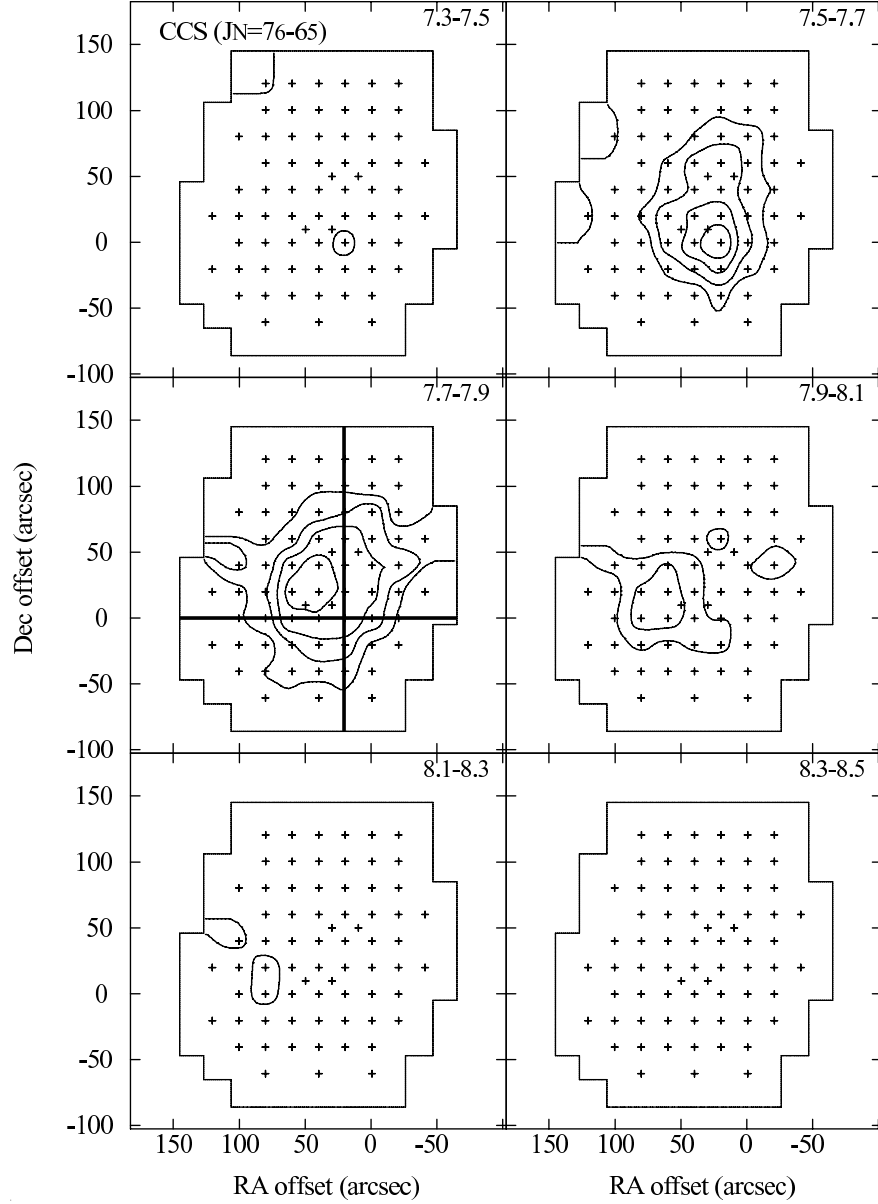


Fig. 7.— Channel maps of the CCS(7<sub>6</sub>–6<sub>5</sub>) line in L492. The velocity range is labeled at the top right corner in each panel. The interval of the contours and the lowest contour are 0.030 K km s<sup>–1</sup> and 0.045 K km s<sup>–1</sup>, respectively. The peak LSR velocity of L492 corresponds to 7.7-7.9 km s<sup>–1</sup>. The position-velocity diagrams shown in Figure 8 are made along the bold solid lines in this panel.

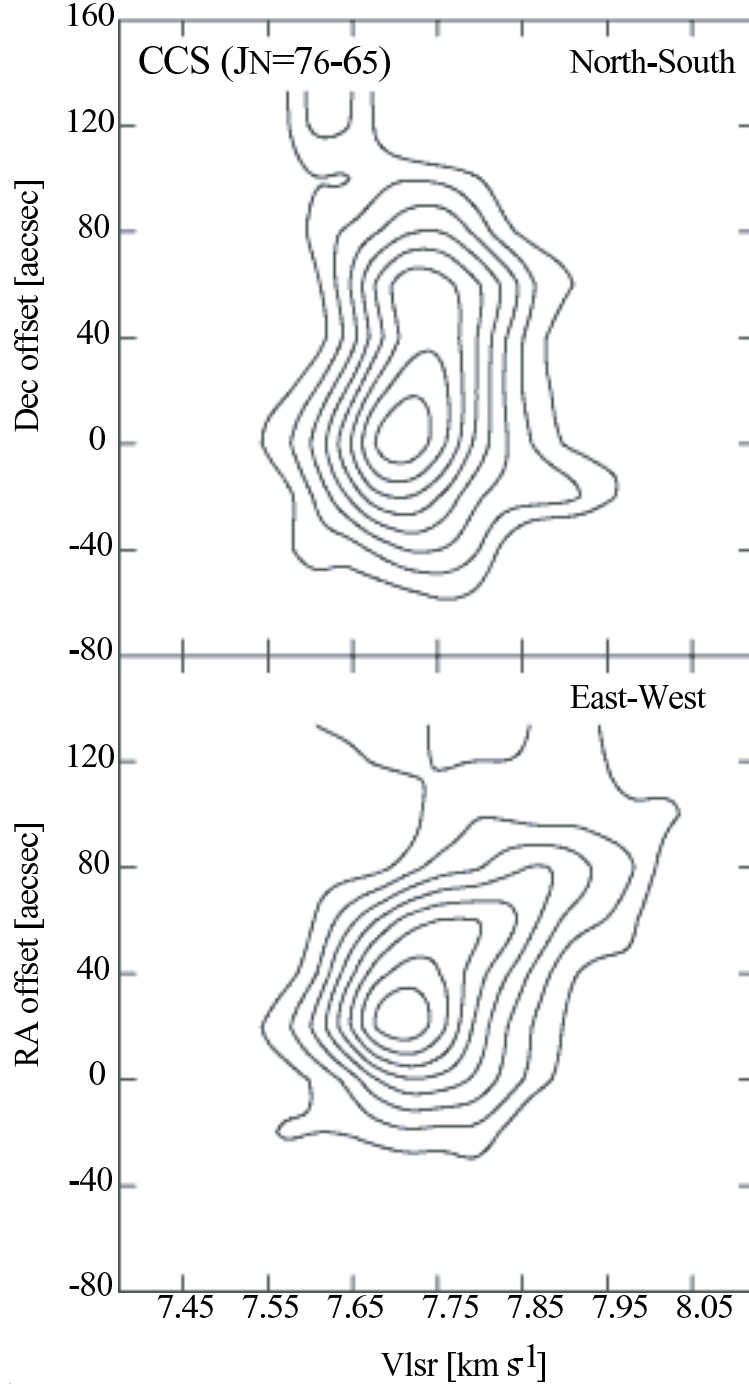


Fig. 8.— Position-velocity (p-v) diagrams of the  $\text{CCS}(J_N=7_6-6_5)$  line. The top panel shows the p-v diagram along the north-south direction at the offset in right ascension of  $20''$ , and the bottom panel shows that along the east-west direction at the offset in declination of  $0''$ , as shown in Figure 7. The interval of the contours and the lowest contour are 0.10 K for both panels.

Table 1. Gauss fit parameters for the observed lines

Transition	Frequency (MHz)	Position	$T_a^*$ (K)	$v_{lsr}$ (km s <sup>-1</sup> )	$\Delta v$ (km s <sup>-1</sup> )	$T_{rms}$ (K)
<sup>13</sup> CO( $J=1-0$ ) <sup>a</sup>	110201.353	(20'',20'')	2.5(12)	7.92(15)	1.6(10)	0.3
C <sup>18</sup> O( $J=1-0$ ) <sup>a</sup>	109782.173	(20'',20'')	1.20(15)	7.69(5)	0.62(13)	0.15
DCO <sup>+</sup> ( $J=1-0$ ) <sup>a</sup>	72039.331	(20'',20'')	0.83(17)	7.70(5)	0.49(13)	0.13
DNC( $J=1-0$ ) <sup>a</sup>	76305.717	(20'',20'')	0.67(17)	7.67(9)	0.73(22)	0.09
H <sup>13</sup> CO <sup>+</sup> ( $J=1-0$ ) <sup>a</sup>	86754.330	(20'',20'')	0.83(10)	7.83(4)	0.61(10)	0.08
HN <sup>13</sup> C( $J=1-0$ ) <sup>a</sup>	87090.859	(20'',20'')	0.47(13)	7.82(10)	0.72(28)	0.07
C <sup>34</sup> S( $J=1-0$ ) <sup>a</sup>	48206.946	(40'',0'')	0.71(17)	7.82(6)	0.48(14)	0.08
C <sup>34</sup> S( $J=2-1$ ) <sup>a</sup>	96412.961	(40'',0'')	0.47(9)	7.74(4)	0.37(8)	0.06
CCS( $J_N=2_1-1_0$ )	22344.030	(40'',0'')	0.69(6)	7.78(3)	0.80(8)	0.03
CCS( $J_N=4_3-3_2$ ) <sup>a</sup>	45379.033	(40'',0'')	1.51(10)	7.73(2)	0.48(4)	0.07
CCS( $J_N=7_6-6_5$ ) <sup>a</sup>	81505.208	(40'',0'')	0.87(20)	7.71(5)	0.42(12)	0.09
C <sub>3</sub> S( $J=4-3$ )	23122.983	(40'',0'')	0.41(6)	7.77(4)	0.59(11)	0.04
HC <sub>3</sub> N( $J=5-4, F=5-5$ )	45488.834	(40'',0'')	0.35(13)	7.76(3)	0.81(7)	0.09
HC <sub>3</sub> N( $J=5-4, F=6-5/5-4/4-3$ ) <sup>a,b</sup>	45490.306	(40'',0'')	2.35(16)	7.76(3)	0.81(7)	0.09
HC <sub>3</sub> N( $J=5-4, F=4-4$ )	45492.106	(40'',0'')	0.21(13)	7.76(3)	0.81(7)	0.09
HC <sub>3</sub> N( $J=9-8$ ) <sup>a</sup>	81881.462	(40'',0'')	1.70(9)	7.73(1)	0.46(3)	0.09
HC <sub>5</sub> N( $J=9-8$ )	23963.901	(40'',0'')	1.00(8)	7.81(3)	0.75(7)	0.03
HC <sub>5</sub> N( $J=17-16$ ) <sup>a</sup>	45264.720	(40'',0'')	1.23(12)	7.76(2)	0.49(6)	0.06
HC <sub>7</sub> N( $J=21-20$ )	23687.898	(0'',0'')	0.18(4)	7.65(6)	0.56(15)	0.02
N <sub>2</sub> H <sup>+</sup> ( $J, F_1, F=1,1,0-0,1,1$ ) <sup>a</sup>	93171.621	(20'',20'')	0.28(10)	7.75(2)	0.44(4)	0.08
N <sub>2</sub> H <sup>+</sup> ( $J, F_1, F=1,1,2-0,1,2$ ) <sup>a</sup>	93171.917	(20'',20'')	0.52(11)	7.75(2)	0.44(4)	0.08
N <sub>2</sub> H <sup>+</sup> ( $J, F_1, F=1,1,1-0,1,0$ ) <sup>a</sup>	93172.053	(20'',20'')	0.48(11)	7.75(2)	0.44(4)	0.08
N <sub>2</sub> H <sup>+</sup> ( $J, F_1, F=1,2,2-0,1,1$ ) <sup>a</sup>	93173.480	(20'',20'')	0.59(10)	7.75(2)	0.44(4)	0.08
N <sub>2</sub> H <sup>+</sup> ( $J, F_1, F=1,2,3-0,1,2$ ) <sup>a</sup>	93173.777	(20'',20'')	0.92(11)	7.75(2)	0.44(4)	0.08
N <sub>2</sub> H <sup>+</sup> ( $J, F_1, F=1,2,1-0,1,1$ ) <sup>a</sup>	93173.967	(20'',20'')	0.40(11)	7.75(2)	0.44(4)	0.08
N <sub>2</sub> H <sup>+</sup> ( $J, F_1, F=1,0,1-0,1,2$ ) <sup>a</sup>	93176.265	(20'',20'')	0.67(10)	7.75(2)	0.44(4)	0.08
NH <sub>3</sub> ( $J, K=1, 1$ ; VH) <sup>a,c</sup>	23692.955	(0'',0'')	0.19(7)	7.87(4)	0.86(10)	0.04
NH <sub>3</sub> ( $J, K=1, 1$ ; H) <sup>a,c</sup>	23693.895	(0'',0'')	0.31(7)	7.87(4)	0.86(10)	0.04
NH <sub>3</sub> ( $J, K=1, 1$ ; M) <sup>a,c</sup>	23694.496	(0'',0'')	0.74(8)	7.87(4)	0.86(10)	0.04
NH <sub>3</sub> ( $J, K=1, 1$ ; L) <sup>a,c</sup>	23695.095	(0'',0'')	0.33(7)	7.87(4)	0.86(10)	0.04
NH <sub>3</sub> ( $J, K=1, 1$ ; VL) <sup>a,c</sup>	23696.037	(0'',0'')	0.24(7)	7.87(4)	0.86(10)	0.04
NH <sub>3</sub> (2,2)	23722.634	(0'',0'')	0.06(2)	7.71(11)	0.63(27)	0.02

Note. — The numbers in parenthesis represent three times the standard deviation in the Gaussian fit in unit of the last significant digits.

<sup>a</sup>Maps of the lines is shown in Figure 1.

<sup>b</sup>Three hyperfine components are blended.

<sup>c</sup>Hyperfine components are blended. Each component is labeled as adopted by Ungerechts et al. (1980) and Figure 5.

Table 2. Results of LVG calculations

Molecule	Transition	$S_{ul}$ <sup>a</sup>	$\mu$ <sup>b</sup> (Debye)	Position	$\tau_0$	$T_{ex}$ (K)	$n(\text{H}_2)$ ( $\times 10^5 \text{cm}^{-3}$ )	$N$ ( $\times 10^{13} \text{cm}^{-2}$ )	Reference
DCO <sup>+</sup>	$J=1-0$	1.00	4.07	(20'',20'')	0.47	7.4	0.90 <sup>c</sup>	0.109	1,2
DNC	$J=1-0$	1.00	3.05	(20'',20'')	1.9	4.4	0.90 <sup>c</sup>	0.56	3,4
H <sup>13</sup> CO <sup>+</sup>	$J=1-0$	1.00	4.07	(20'',20'')	0.82	5.9	0.90 <sup>c</sup>	0.137	1,2
HN <sup>13</sup> C	$J=1-0$	1.00	3.05	(20'',20'')	2.2	3.9	0.90 <sup>c</sup>	0.44	3,4
C <sup>34</sup> S	$J=1-0$	1.00	1.96	(40'',0'')	0.20	8.6	0.90	0.38	5,6
	$J=2-1$	2.00	1.96	(40'',0'')	0.79	4.7			
CCS	$J_N=4_3-3_2$	3.97	2.81	(40'',0'')	0.43	9.0	0.68	1.61	7,8,9
	$J_N=7_6-6_5$	6.97	2.81	(40'',0'')	0.54	7.1			

<sup>a</sup>Intrinsic line strength.

<sup>b</sup>Dipole moment.

<sup>c</sup>The H<sub>2</sub> density derived from the C<sup>34</sup>S data is assumed.

References. — 1: Haese & Woods (1979); 2: Monteiro (1985); 3: Blackman et al. (1976); 4: Green & Thaddeus (1974); 5: Winnewisser & Cook (1968); 6: Green & Chapman (1978); 7: Murakami (1990); 8: Yamamoto et al. (1990); 9: Wolkovitch et al. (1997)

Table 3. Results of LTE calculations

Molecule	Transition	$S_{ul}^a$	$\mu^b$ (Debye)	Position	$\tau_0$	$T_{ex}$ (K)	$N$ ( $\times 10^{13} \text{cm}^{-2}$ )	NOTE	Reference
$^{13}\text{CO}$	$J=1-0$	1.00	0.11	(20'',20'')	4.0	8.3	1960	$^{13}\text{CO}/\text{C}^{18}\text{O}=7.3$	1
$\text{C}^{18}\text{O}$	$J=1-0$	1.00	0.11	(20'',20'')	0.64	8.3	310	$^{13}\text{CO}/\text{C}^{18}\text{O}=7.3$	1
$\text{CCS}$	$J_N=4_3-3_2$	3.97	2.81	(40'',0'')	3.4	5.0	5.3	$T_{ex}$ fixed	2,3
$\text{C}_3\text{S}$	$J=4-3$	4.00	3.64	(40'',0'')	0.21	5.5	0.55	$T_{ex}$ fixed	2,3
$\text{HC}_3\text{N}$	$J=5-4$	5.00	3.72	(40'',0'')	8.8	6.4	17.2	hf fit <sup>c</sup>	4
$\text{HC}_5\text{N}$	$J=17-16$	17.00	4.33	(40'',0'')	0.65	6.5	4.1	$T_{ex}$ fixed	5
$\text{HC}_7\text{N}$	$J=21-20$	21.00	4.82	(0'',0'')	0.03	10.0	0.32	$T_{ex}$ fixed	6
$\text{N}_2\text{H}^+$	$J=1-0$	1.00	3.40	(20'',20'')	6.1	4.9	0.66	hf fit <sup>c</sup>	7
$\text{NH}_3$	(1, 1)	1.50	1.46	(0'',0'')	2.3	4.1	34	hf fit <sup>c</sup> , $T_{rot}=10 \text{ K}$	8

<sup>a</sup>Intrinsic line strength.

<sup>b</sup>Dipole moment.

<sup>c</sup>Total optical depth and excitation temperatures are derived from a simultaneous fit to the hyperfine (hf) components.

References. — 1: Goorvitch (1994); 2: Murakami (1990); 3: Yamamoto et al. (1990); 4: Lafferty & Lovas (1978); 5: Alexander et al. (1976); 6: Botschwina et al. (1997); 7: Havenith et al. (1990); 8: Cohen & Poynter (1974)



Table 4. Column densities of the selected molecules in unit of  $10^{13} \text{ cm}^{-2}$

Molecule	L492	L1495B	L1521B	L1521E	TMC-1	Taurus	Others
C <sup>34</sup> S	0.38	...	0.56 <sup>a</sup>	1.25 <sup>a</sup>	0.73 <sup>a</sup>	0.17-2.18 <sup>a</sup>	0.08-0.68 <sup>a</sup>
CCS	5.3 <sup>b</sup>	1.44 <sup>c</sup>	3.6 <sup>d</sup>	2.8 <sup>c</sup>	6.6 <sup>d</sup>	<0.09-6.6 <sup>d</sup>	<1.1-1.51 <sup>d</sup>
C <sub>3</sub> S	0.55	0.68 <sup>e,f</sup>	1.6 <sup>e</sup>	1.4 <sup>g</sup>	1.3 <sup>d</sup>	0.42-1.3 <sup>d</sup>	...
HC <sub>3</sub> N	17.2	2.1 <sup>e</sup>	4.1 <sup>d</sup>	2.3 <sup>g</sup>	17.1 <sup>d</sup>	<0.07-17.1 <sup>d</sup>	<0.07-1.35 <sup>d</sup>
HC <sub>5</sub> N	4.1	0.52 <sup>e</sup>	1.2 <sup>e</sup>	0.46 <sup>g</sup>	5.6 <sup>d</sup>	<0.14-5.6 <sup>d</sup>	<0.17-1.07 <sup>d</sup>
HC <sub>7</sub> N	0.32	...	0.24 <sup>h</sup>	...	1.4 <sup>h</sup>	0.08-1.4 <sup>h</sup>	...
NH <sub>3</sub>	34	5.5 <sup>e</sup>	12.6 <sup>e</sup>	7.3 <sup>g</sup>	19 <sup>d</sup>	<2-107 <sup>d</sup>	<3-112 <sup>d</sup>
N <sub>2</sub> H <sup>+</sup>	0.66	<0.17 <sup>e</sup>	<0.19 <sup>e</sup>	<0.14 <sup>g</sup>	0.74 <sup>i</sup>	0.3-1.3 <sup>j</sup>	0.14-2.7 <sup>j</sup>
H <sup>13</sup> CO <sup>+</sup>	0.137	0.046 <sup>c</sup>	0.063 <sup>c</sup>	0.106 <sup>c</sup>	0.14 <sup>k</sup>	0.038-0.164 <sup>l</sup>	<0.0110-0.126 <sup>l</sup>
C <sup>18</sup> O	310	190 <sup>m</sup>	300 <sup>m</sup>	170 <sup>m</sup>	330 <sup>k</sup>	60-520 <sup>l</sup>	30-700 <sup>l</sup>

Note. — Positions for the cores are as follows: L492:  $\alpha_{2000} = 18^h 15^m 46^s .1$ ,  $\delta_{2000} = -03^\circ 46' 13''$  and Tables 2 and 3; L1495B:  $\alpha_{2000} = 04^h 15^m 36^s .5$ ,  $\delta_{2000} = +28^\circ 47' 06''$ ; L1521B:  $\alpha_{2000} = 04^h 24^m 12^s .7$ ,  $\delta_{2000} = +26^\circ 36' 53''$ ; L1521E:  $\alpha_{2000} = 04^h 29^m 16^s .5$ ,  $\delta_{2000} = +26^\circ 13' 50''$ ; TMC-1:  $\alpha_{2000} = 04^h 41^m 42^s .5$ ,  $\delta_{2000} = +25^\circ 41' 27''$ .

<sup>a</sup>Hirota et al. (1998).

<sup>b</sup>The LTE value is employed here for consistency with other results.

<sup>c</sup>Hirota et al. (2001).

<sup>d</sup>Suzuki et al. (1992).

<sup>e</sup>Hirota et al. (2004).

<sup>f</sup>Position is (80'',40'') offset from the reference position.

<sup>g</sup>Hirota et al. (2002).

<sup>h</sup>Cernicharo et al. (1986).

<sup>i</sup>Hirahara et al. (1995).

<sup>j</sup>Caselli et al. (2002a).

<sup>k</sup>Pratap et al. (1997).

<sup>l</sup>Butner et al. (1995).

<sup>m</sup>Myers et al. (1983).

Table 5. Molecular abundance ratios as an indicator of chemical evolution

Molecule	L1495B	L1521B	L1521E	TMC-1(CP)	L492	L1498	L1544
DNC/HN <sup>13</sup> C	<0.66 <sup>a</sup>	0.70 <sup>a</sup>	0.66 <sup>b</sup>	1.25 <sup>c</sup>	1.27	1.91 <sup>a</sup>	3.0 <sup>c</sup>
DCO <sup>+</sup> /H <sup>13</sup> CO <sup>+</sup>	1.05 <sup>a</sup>	1.10 <sup>a</sup>	0.63 <sup>a</sup>	0.77 <sup>d</sup>	0.80	2.7 <sup>e</sup>	3.1-9.2 <sup>f</sup>
NH <sub>3</sub> /CCS	3.8 <sup>a,g</sup>	3.5 <sup>g,h</sup>	2.6 <sup>a,b</sup>	2.9 <sup>h</sup>	6.5	25 <sup>h</sup>	15 <sup>h,i</sup>

Note. — Positions for the cores are as follows: L1498:  $\alpha_{2000} = 04^h 10^m 51^s.5$ ,  $\delta_{2000} = +25^\circ 09' 58''$ ; L1544:  $\alpha_{2000} = 05^h 04^m 16^s.6$ ,  $\delta_{2000} = +25^\circ 10' 48''$ .

<sup>a</sup>Hirota et al. (2001).

<sup>b</sup>Hirota et al. (2002).

<sup>c</sup>Hirota et al. (2003).

<sup>d</sup>Turner (2001).

<sup>e</sup>Butner et al. (1995).

<sup>f</sup>Caselli et al. (1999).

<sup>g</sup>Hirota et al. (2004).

<sup>h</sup>Suzuki et al. (1992).

<sup>i</sup>Position is (-19'',60'') offset from the reference position.

Table 6. Evolutionary scenario of dark cloud cores

Item	L1495B	L1521B	L1521E	TMC-1(CP)	L492	L1498	L1544
Gas-phase molecular abundance							
DNC/HN <sup>13</sup> C <sup>a</sup>	Y	Y	Y	Y	Y	E	E
DCO <sup>+</sup> /H <sup>13</sup> CO <sup>+</sup> <sup>a</sup>	Y	Y	Y	Y	Y	E	E
N <sub>2</sub> D <sup>+</sup> /N <sub>2</sub> H <sup>+</sup> <sup>b</sup>	?	?	Y	Y	E	E	E
NH <sub>3</sub> /CCS <sup>a</sup>	Y	Y	Y	Y	I	E	E
Degree of depletion							
Depletion factor of CO <sup>b</sup>	?	?	Y	?	I	I	E
Map structure of CS and CCS <sup>c</sup>	Y	Y	Y	Y	I?	E	E
Kinematics							
Signature of infall <sup>d</sup>	?	Y	Y	Y	E	E	E

Note. — Y, I, and E indicates young, intermediate, and evolved, respectively.

<sup>a</sup>Table 5

<sup>b</sup>Crapsi et al. (2005)

<sup>c</sup>Hirota et al. (2002, 2004); Tafalla et al. (2002); Tafalla & Santiago (2004)

<sup>d</sup>Lee et al. (1999, 2001); Crapsi et al. (2005)